



Lateral-torsional buckling strength of corrugated web girders – Experimental study

B. Jäger^{*}, L. Dunai, B. Kövesdi

Budapest University of Technology and Economics, Faculty of Civil Engineering, Department of Structural Engineering, H-1111 Budapest, Műegyetem rkp. 3, Hungary

ARTICLE INFO

Keywords:

Corrugated web
Trapezoidal corrugation
Lateral-torsional buckling
Local flange buckling
Bending moment resistance

ABSTRACT

Current standards and specifications do not provide specific design methods to determine the lateral-torsional buckling (LTB) strength of girders with trapezoidally corrugated web. In the international literature there are some previous investigations available focusing on the LTB strength of corrugated web girders. Based on numerical calculations analytical solutions have been derived in the past, however, there is a lack of experimental test results to prove or improve these design proposals. The authors performed an extensive experimental research program including eleven large-scale test specimens. All the test girders have different flange sizes, beside, having the same corrugation profile. The test specimens are loaded by pure in-plane bending having simply supported boundary conditions. The tested specimens have limited warping and rotational restraint at the supports. No web distortional type failure is observed. During the tests the longitudinal strains are captured in characteristic cross-sections and the displacements in vertical and lateral directions are measured as well as the rotation of the mid-span cross-section. The measured LTB strength of the test specimens is compared with existing analytical proposals regarding corrugated web girders and the differences are evaluated. It is observed that the imperfections have key role in the LTB behavior. Based on the experimental results buckling curve “b” from Eurocode 3 is preliminary proposed for the determination of the lateral-torsional buckling strength of trapezoidally corrugated web girders. The executed test program gives useful background to further numerical studies.

1. Introduction

Corrugated web girders are increasingly used in the structural engineering praxis due to their numerous favorable properties, such as lower dead load, increased shear buckling strength, special structural behavior called “accordion effect” which makes the design simpler compared to those of girders with flat web. The local and global member stability has great importance in the design of these girders. In the international literature the effect of local stability on cross-sectional resistances, namely the (i) bending moment resistance, (ii) shear buckling resistance and (iii) resistance against transverse force have been extensively studied by researchers in the past and there are accurate design models available for the determination of these resistances.

The global member stability, namely the lateral-torsional buckling strength of corrugated web girders was first investigated by Lindner [1]. Since then some researchers studied the elastic critical moment and ultimate strength of corrugated web girders. There is an agreement between researchers that the elastic critical moment of girders with

corrugated web is greater than those of with flat web. The increment has been, however, considered in different ways by attributing to different cross-sectional properties. Furthermore, the ultimate lateral-torsional buckling strength was investigated mainly by nonlinear FE (finite element) analysis in the past; the number of available test results is limited. The current paper focuses on the experimental study of 11 large-scale test specimens investigating the lateral-torsional buckling resistance of corrugated web girders. Based on the test results, the previous design proposals are compared, evaluated and a preliminary design buckling curve is proposed for the determination of the lateral-torsional buckling strength of trapezoidally corrugated web girders. The applied notations in the paper are given in Fig. 1.

2. Literature review

2.1. Investigations on the elastic critical moment

The elastic critical moment of a conventional flat web girder sub-

^{*} Corresponding author.

E-mail address: jager.bence@emk.bme.hu (B. Jäger).

<https://doi.org/10.1016/j.istruc.2022.07.053>

Received 20 March 2022; Received in revised form 9 July 2022; Accepted 20 July 2022

Available online 26 July 2022

2352-0124/© 2022 The Author(s). Published by Elsevier Ltd on behalf of Institution of Structural Engineers. This is an open access article under the CC BY license (<http://creativecommons.org/licenses/by/4.0/>).

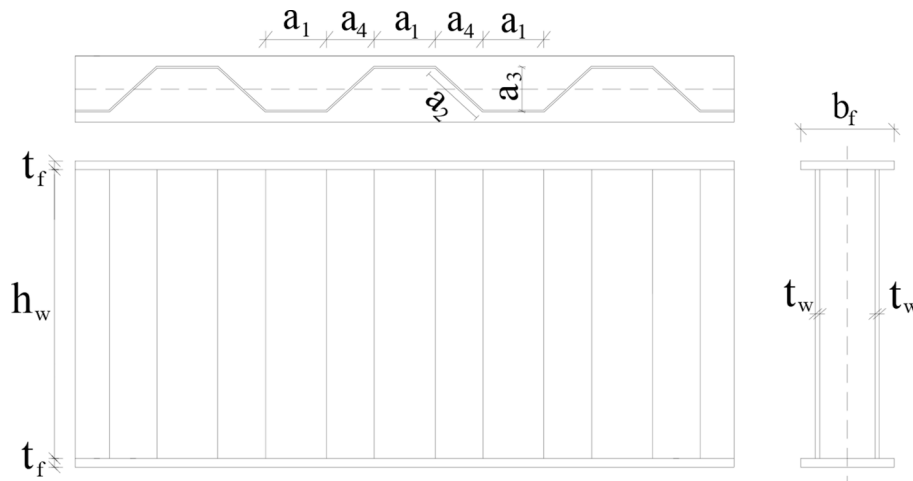


Fig. 1. Applied notations.

jected to uniform bending moment can be calculated by Eq. (1) according to EN1993-1-1 [2] and Timoshenko and Gere [3].

$$M_{cr} = \frac{\pi}{k \cdot L} \sqrt{EI_z \left[\left(\frac{\pi}{k_w \cdot L} \right)^2 EI_w + GI_t \right]} \quad (1)$$

In the above equation, L is the span of the girder, E is the elastic modulus, G is the shear modulus, I_z is the moment of inertia about the minor axis, I_t is the torsional constant, I_w is the warping constant, k is the effective length factor about the weak axis rotation and k_w is the effective length factor with respect to warping.

In the past, several researchers found that the elastic critical moment of the girders with trapezoidally corrugated web and their ultimate strength are greater than that of girders with conventional flat web (Sayed-Ahmed [4], Moon et al. [5], Nguyen et al. [6], Zhang et al. [7], Larsson and Persson [8], Ilanovsky [9]). The increase in the elastic critical moment has been, however, attributed to different sectional properties by different authors. Most of the researchers agree that the web contribution should be ignored in the moment of inertias about the strong and weak axes, but there are contradictions in the consideration of the increased elastic critical moment. Firstly, Lindner [1] suggested an additional term with a correction factor c_w in the warping constant given by Eqs. 2–4 for double symmetric sections in order to consider the greater performance ($c_1 = 8$, $c_2 = 25$); where $I_{w,flat}$ is the warping constant of flat web girder.

$$I_w = I_{w,flat} + c_w \frac{L^2}{E\pi^2} \quad (2)$$

$$c_w = \frac{a_3^2 \cdot (h_w + t_f)^2}{c_1 \cdot u_x \cdot (a_1 + a_4)} \quad (3)$$

$$u_x = \frac{(h_w + t_f)}{2 \cdot G \cdot a_1 \cdot t_w} + \frac{(h_w + t_f)^2 \cdot (a_1 + a_4)^3}{c_2 \cdot a_1^2 \cdot E \cdot b_f \cdot t_f^3} \quad (4)$$

Moon et al. [5], Nguyen et al. [6], Zhang et al. [7] and Ibrahim [10] also proposed that the greater performance should be taken into account in the warping constant and new additional terms were developed. Larsson and Persson [8] performed a notable FE study and found that the proposal of Lindner [1] gives the best approximation to the numerical results. However, this additional term depends on the girder length which is not possible for a sectional constant. Therefore, they substituted the Lindner's proposal into Eq. (1) in order to rearrange the additional term to the torsional constant according to Eq. (5).

$$I_t = I_{t,flat} + \frac{c_w}{G} \quad (5)$$

The appropriateness of Eq. (5) was confirmed by Lopes et al. [11] and they proposed a slightly modified correction factor c_w for trapezoidally and sinusoidally corrugated web girders ($c_1 = 22$, $c_2 = 300$ in Eqs. 3–4) based on FE analysis. In addition, Guo and Papangelis [12] comparatively studied the torsional behavior of trapezoidally corrugated and flat web girders subjected to uniform and non-uniform torsion. Their FE analysis showed that the torsional constant of girders with corrugated web is significantly greater than those of with flat web, however, there is just a minor difference between the warping constant. This statement confirms the accordion effect since the presence of normal stresses in the web panel is negligible.

Other proposals were also applied for the consideration of the greater performance by using equivalent web thickness (Sayed-Ahmed [4]), reduced shear modulus (Moon et al. [5], Nguyen et al. [6], Ibrahim [10], Kazemi [13]) or using a simple multiplication factor on the elastic critical moment of flat web girders (Ilanovsky [9]).

In addition, some research activities were focusing on different loading and boundary conditions as well. Nguyen et al. numerically studied different end restraint conditions of simply supported girders considering (i) the concentrated load height effect for three-point-bending loading condition [14], (ii) the tapered configuration [15], and (iii) the different moment gradients along the girder length [16]. The effect of linear moment gradient was also studied by Moon et al. [17] and Lopes et al. [11]. Based on the FE results new moment modification factors are proposed on the elastic critical moment for corrugated web girders.

2.2. Investigations on the lateral-torsional buckling strength

The ultimate lateral-torsional buckling strength of corrugated web girders has been studied through only a few number of experimental tests and some nonlinear FE analysis by different researchers. The lateral-torsional buckling strength was experimentally investigated under three-point-bending by Kubo and Watanabe [18] on nine trapezoidally corrugated web girders and under four-point bending by Elkawas et al. [19], and Hannebauer [20] and Pimenta et al. [21] on three and four sinusoidally corrugated web girders, respectively. In addition, Zhang et al. [22] tested four sinusoidally corrugated web girders using a cantilever arrangement with concentrated load introduction at the end of the cantilever.

According to EN1993-1-1 [2] the reduction factor (χ_{LT}) for the lateral-torsional buckling strength for rolled sections or equivalent welded sections with flat web may be calculated by Eqs. 6–8, where a_{LT} is the imperfection factor (for different buckling curves: $a - 0.21$, $b - 0.34$, $c - 0.49$, $d - 0.76$), $\bar{\lambda}_{LT}$ is the relative slenderness, β is the

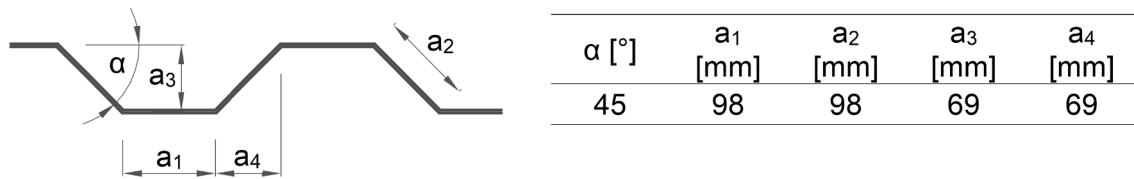


Fig. 2. Applied trapezoidal corrugation profile.

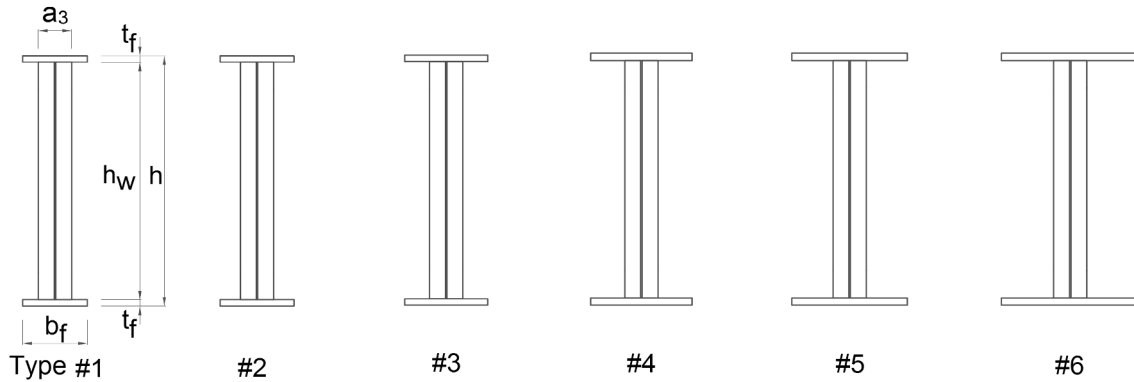


Fig. 3. Cross-sectional layout of specimen's geometry.

multiplication factor and $\bar{\lambda}_{LT,0}$ is the relative slenderness limit. The standard suggests to use buckling curve *d* if the depth-to-width ratio of the section is greater than 2; otherwise the buckling curve *c* shall be used. In Eq. (8) M_y is the cross-sectional bending moment resistance considering the local flange buckling as given by Eq. (9).

$$\chi_{LT} = \frac{1}{\Phi_{LT} + \sqrt{\Phi_{LT}^2 - \beta \bar{\lambda}_{LT}^2}} \text{ but } \chi_{LT} \leq \min \left(1.0; \frac{1}{\bar{\lambda}_{LT}^2} \right) \quad (6)$$

$$\Phi_{LT} = \frac{1 + \alpha_{LT} \cdot (\bar{\lambda}_{LT} - \bar{\lambda}_{LT,0}) + \beta \bar{\lambda}_{LT}^2}{2} \quad (7)$$

$$\bar{\lambda}_{LT} = \sqrt{\frac{M_y}{M_{cr}}} \quad (8)$$

Nonlinear FE analyses have been conducted by Moon et al. [5,17] and it is concluded that the use of the buckling curve *b* ($\beta=1.0$ and $\bar{\lambda}_{LT,0} = 0.2$) of EN1993-1-1 results in conservative solutions for trapezoidally corrugated web girders. Ibrahim [10] performed nonlinear FE analysis on trapezoidally corrugated web girders with unequal flanges and found that the lateral-torsional buckling curve *d* of EN1993-1-1 is applicable using $\beta = 0.75$ and $\bar{\lambda}_{LT,0} = 0.4$; this is confirmed by Hassanein et al. [23] who numerically studied high-strength girders having unequal flanges. Elkawas et al. [24] numerically studied high-strength steel trapezoidally corrugated web girders and found that the lateral-torsional buckling

curve *a* could be applicable using $\beta = 0.75$ and $\bar{\lambda}_{LT,0} = 0.4$. This was confirmed by Shao et al. [25] who numerically investigated the LTB strength of high-strength steel girders. According to their latest result [26] the buckling curve *a* may be applicable for corrugated web girders.

The authors performed an imperfection sensitivity study using nonlinear FE analysis where artificial initial geometric imperfections and residual stresses are considered [27]. These results showed that both geometric and structural imperfections shall be considered in the finite element method based design and two residual stress patterns are proposed for narrow and wide flange beams. The available test results are, however, very limited to prove the applicability of any of the previous proposals. Therefore, a new experimental research program is designed, executed and presented in the current paper.

3. Experimental research program

3.1. Test specimens

Experimental research program is performed in 2018 at the Budapest University of Technology and Economics, Department of Structural Engineering in Hungary. In the frame of the research program 11 large-scale test specimens are investigated by four-point-bending condition. Six different girder geometries having different flange sizes and the same trapezoidal corrugation profile are investigated. Further 5 specimens are used for test duplications investigating the accuracy of the results. The

Table 1
Measured geometrical and material properties of the test specimens.

Specimen	t_f (mm)	b_f (mm)	t_w (mm)	h (mm)	h_w (mm)	t_s (mm)	f_{yf} (MPa)	f_{uf} (MPa)	f_{yw} (MPa)	f_{uw} (MPa)
1/1	13.8	139	6	547.0	519.3	10	357	528	289	379
1/2	14.1	140	6	545.5	517.3	10	357	528	289	379
2/1	14.0	158	6	548.5	520.6	10	357	528	289	379
2/2	14.0	162	6	546.5	518.4	10	357	528	289	379
3/1	14.0	181	6	546.5	518.5	14	357	528	289	379
3/1	14.0	179	6	548.0	520.0	14	357	528	289	379
4/1	16.7	219	6	553.0	519.6	14	379	534	289	379
5/1	16.5	250	6	552.0	519.0	14	379	534	289	379
5/2	16.6	250	6	550.0	516.8	14	379	534	289	379
6/1	15.9	300	6	551.0	519.1	16	372	520	289	379
6/2	16.1	300	6	550.0	517.9	16	372	520	289	379

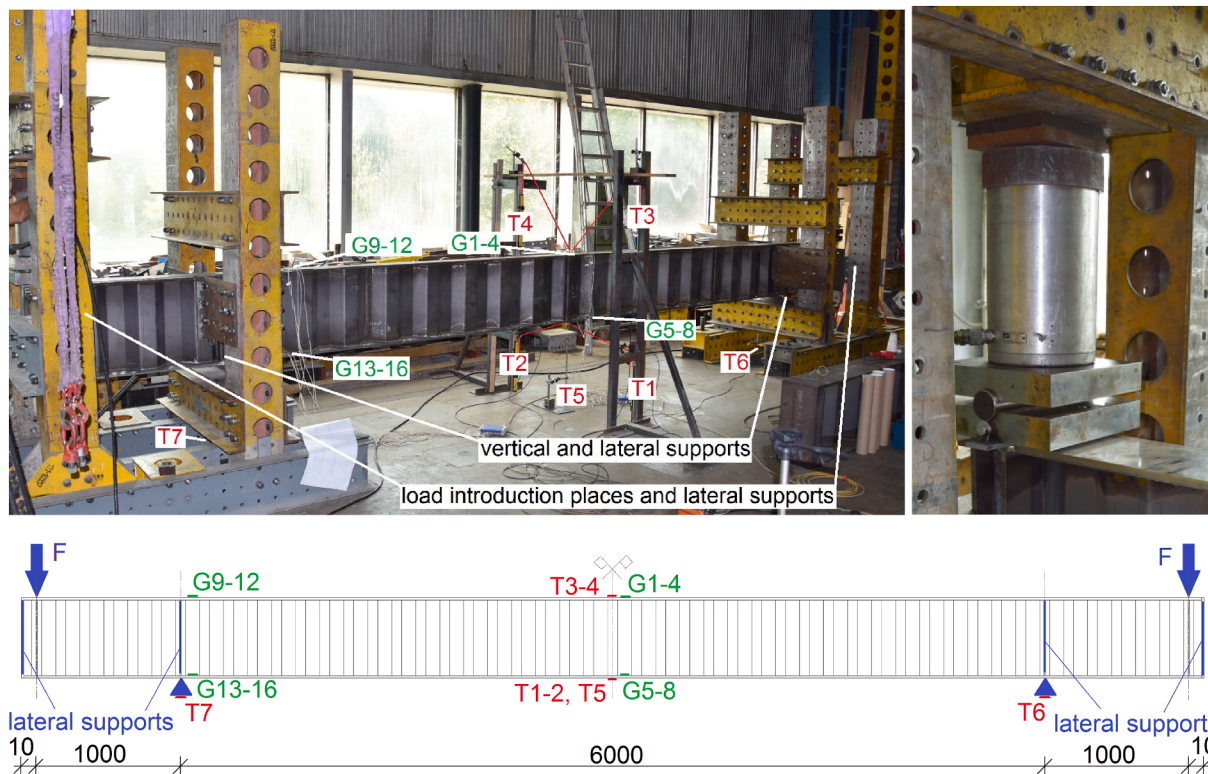


Fig. 4. Test setup and location of measuring devices.

measured geometrical and material properties of the tested girders and the notations are summarized in Figs. 2 and 3 and in Table 1. For all the specimens the widths of the parallel and inclined web folds are equal ($a_1 = a_2 = 98$ mm) as mainly used in bridges with a corrugation angle of 45° .

Fig. 3 presents the scaled drawings of the six specimen types having different flange sizes; the numbering of the girders is set accordingly in the order of increasing flange sizes. The nominal flange thickness (t_f) of specimen type #1, #2 and #3 is 14 mm, while it is 16 mm for specimen type #4, #5 and #6 tabulated in the second column of Table 1. The nominal flange widths (b_f) are 140, 160, 180, 220, 250, and 300 mm, respectively. The thickness of the web (t_w) is 6 mm for all specimens with a nominal web depth (h_w) of 520 mm. At the load introduction and support locations vertical stiffeners are placed with a nominal thickness (t_s) of 10 to 16 mm. The specimens are designed to cover a wide range of different LTB slenderness ratios to characterize the lateral-torsional buckling behavior of corrugated web girders. The steel material has a prescribed steel grade of S355 for flanges and S235 for the web with a nominal yield strength of 355 MPa and 235 MPa, respectively. The

material properties are evaluated by coupon tests according to ISO 6892-1 [28]. Results can be found in the last columns of Table 1 regarding the flange yield (f_{yf}) and tensile strength (f_{tuf}) and web yield (f_{yw}) and tensile strength (f_{tuw}), respectively.

3.2. Test setup

The applied test arrangement is presented in Fig. 4. The general purpose of the test layout is to apply large clear span (6000 mm), ensuring large buckling length. The total length of the tested girders is 8.2 m. The specimens are vertically supported at the cross-sections 1100 mm from both ends. The concentrated vertical forces are introduced at the end cross-sections (100 mm from both ends) creating a four-point-bending loading condition with lever arms of 1000 mm (both ends can displace downwards). The load is produced by two hydraulic jacks with maximum loading capacities of 1000 kN. The concentrated transverse force is introduced through rigid steel load transfer elements placed on the upper flange. The girders are laterally supported at the vertical



Fig. 5. Strain gauge distribution on the top flange and shear strengthening of cantilever parts.

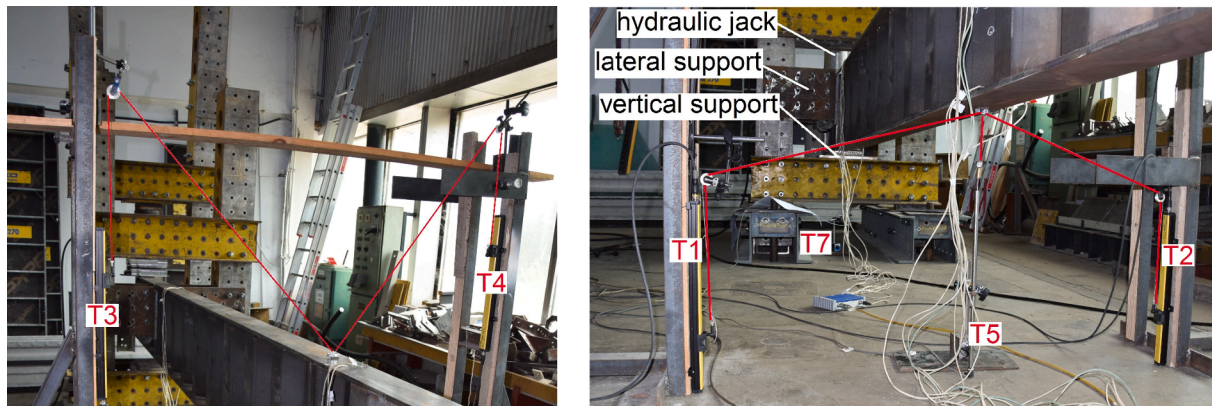


Fig. 6. Measurement system of the mid-span cross-section.

Table 2
Orientation and location of measurement devices.

Notation	Device	Orientation	Location
T1, T2	linear variable displacement transducers	diagonal	bottom flange at mid-span
T3, T4		diagonal	top flange at mid-span
T5		vertical	bottom flange at mid-span
T6, T7	strain gauges	longitudinal	support motion
G1-4			upper surface of top flange at mid-span
G5-8			upper surface of bottom flange at mid-span
G9-12			upper surface of top flange at support
G13-16			upper surface of bottom flange at support

supports and load introduction places in order to restrain the out-of-plane rotation, thus to anchor the transverse bending moment. In addition, the specimens are strengthened by vertical stiffeners at the locations of vertical supports and load introduction places in order to avoid local failure. By this setup the twist and warping are restrained, so thus the torsional moment is anchored, and bimoment can develop. Furthermore, the two 1000 mm long cantilevers are strengthened by braces as shown in Fig. 5 to improve the shear strength and avoid premature shear buckling failure of the test girders; this strengthening also helps the warping restraint. The specimens are equipped by linear variable displacement transducers (LVDTs) and strain gauges which are shown in Figs. 4–6 and tabulated in Table 2. During the tests the 3 DOFs movement of the middle cross-section is captured, namely the (i) deflection, (ii) lateral displacement, and (iii) rigid body rotation by using a rigid frame equipped with four LVDTs denoted by T1–4. These LVDTs are attached in one point to the specimen's bottom (T1–2) and top (T3–4) flanges with diagonal wiring via steel rollers. The diagonal wires create two scalene triangles with changing edges during the tests. Since, four LVDTs are attached the measurement system is overdetermined for the derivation of the 3 DOFs movement giving a control option for the evaluation. Beside, an additional vertically placed LVDT is used denoted by T5 in order to control T1–4 in elastic state.

Strains are also measured at characteristic points of the specimens by strain gauges denoted by G1–16 in Figs. 4 and 5 and Table 2. The strain gauges are attached to the upper surfaces of the top (G1–4 and G9–12) and bottom (G5–8 and G13–16) flanges at the middle of the first parallel folds from the middle and vertical support cross-sections. At each location four strain gauges are placed along the flange width in equal distances placed from the flange edges.

Table 3
Ultimate strengths obtained in the tests.

Specimen	c_f/t_f	flange class	M_{test} (kNm)	M_y (kNm)	M_{test}/M_y	failure modes ¹
1/1	7.5	2	297.4	366.2	0.81	LTB
1/2	7.4	2	321.8	374.7	0.86	LTB
2/1	8.1	2	366.0	421.2	0.87	LTB
2/2	8.2	3	351.9	421.4	0.84	LTB
3/1	8.9	3	449.2	481.4	0.93	LTB
3/1	8.8	3	419.9	478.4	0.88	LTB
4/1	8.6	3	720.0	743.8	0.97	LTB
5/1	9.7	3	795.3	837.7	0.95	LTB → LFB
5/2	9.6	3	844.5	841.5	1.00	LTB → LFB
6/1	11.6	4	972.7	932.4	1.04	LFB + LTB
6/2	11.5	4	977.0	945.4	1.03	LFB + LTB

1. LTB = lateral-torsional buckling, LFB = local flange buckling.

3.3. Testing procedure

Before testing, the spatial coordinates of the rigid frame measurement system are determined by geodetic triangulation calculations using a total station theodolite from three points to reach high accuracy. Each specimen is loaded under static load (~ 0.1 kN/s). During the loading process up- and unloading loops are executed five times by equal loading steps until reaching around 60 % of the predicted ultimate load carrying capacity to determine the elastic response of the structure and to determine the stiffness of the analyzed girders in the elastic domain. The applied hydraulic jacks are synchronized, they are connected to the same hydraulic system. The measured load–displacement curves of the test specimens are measured during testing and the buckling shapes and the ultimate failure modes are documented on photos to evaluate the results and to compare them by FE simulations. During the tests displacement control is applied and the post-buckling ranges are also studied. After performing the tests steel plate pieces are cut out from the undamaged flange and web parts of each specimen for material testing.

4. Test results

4.1. Overall results and failure modes

The observed ultimate loads and failure modes are presented in Table 3. The cross-section classes of the flanges are 2, 3 and barely 4 according to EN1993-1-1 [2] which validity is proved for trapezoidally corrugated web girders by the authors [29,30]. The cross-sectional bending moment resistances (M_y) are calculated by neglecting the web contribution and by considering only the Steiner's terms as a simplification according to Eqs. 9–12 (EN1993-1-5 [31]) for double symmetric sections; where ρ is the reduction factor accounting for local flange buckling based on the effective width method for class 4 flanges



Fig. 7. Lateral-torsional buckling failure (LTB) of specimens.

proposed by the authors [30]. In Eq. (10) c_f is the large flange outstand, η considers the flange-to-web thickness ratio presented by Eq. (11) and R is the enclosing effect of the web corrugation presented by Eq. (12). The latest represents the supporting effect of the web panel to the flange by its geometrical layout. It is to be noted that the reduction due to local flange buckling is only 2 % and 1.5 % for specimens 6/1 and 6/2, respectively.

$$M_y = b_f \cdot (\rho \cdot t_f) \cdot f_{yf} (h_w + t_f) \quad (9)$$

$$\rho = \left(14 \cdot \sqrt{\frac{f_{yf}}{235}} \cdot \frac{t_f}{c_f} \right)^\beta \leq 1.0 \text{ where } \beta = 5 \cdot \eta \cdot R \cdot \left(\frac{a_4}{a_3} \right)^\eta \text{ and } 0.5 \leq \beta \leq 1.0 \quad (10)$$

$$\eta = 0.45 + 0.06 \cdot \frac{t_f}{t_w} \quad (11)$$

$$R = \frac{(a_1 + a_4) \cdot a_3}{(a_1 + 2 \cdot a_4) \cdot b_f} \quad (12)$$

The comparison of the measured LTB resistances and the calculated cross-sectional bending moment resistances are given in Table 3. The failure modes for all specimens are rigid cross-sectional movement and no distortional type failure of the web appeared during the tests. The lateral-torsional buckling failure of each type of specimen is presented in Fig. 7. For specimen types #1, #2, #3 and #4 pure lateral-torsional buckling failure (LTB) occurred, while in the case of specimen type #5 the lateral-torsional buckling is followed by local flange buckling (LTB → LFB) in the post-buckling range. In the case of specimen type #6 the lateral-torsional buckling and local flange buckling are coupled at ultimate load level (LFB + LTB). Fig. 7e and 7f present the combined LTB and LFB type failures.

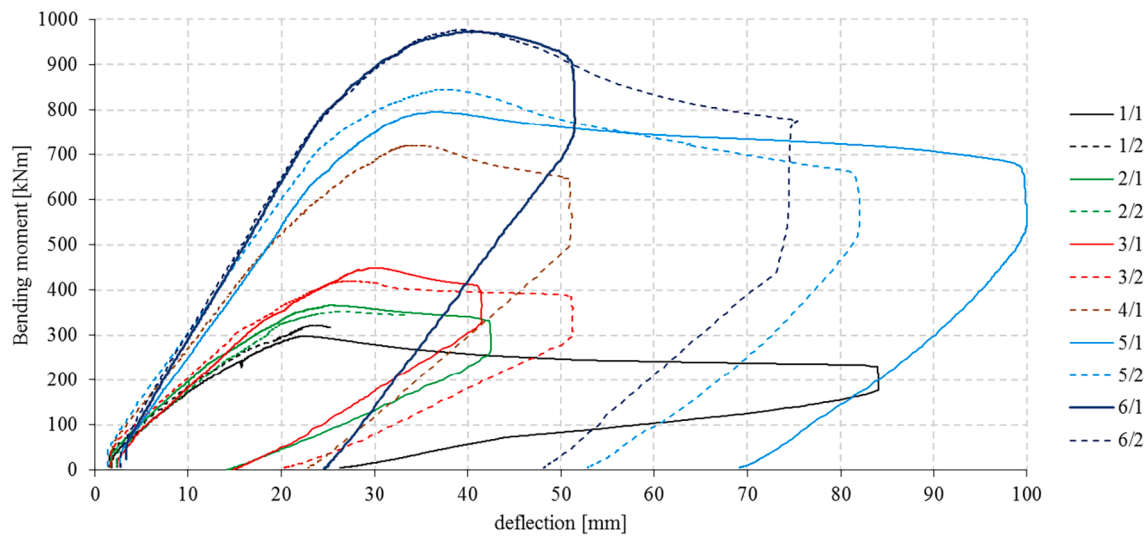


Fig. 8. Moment – deflection diagrams of the middle cross-sections.

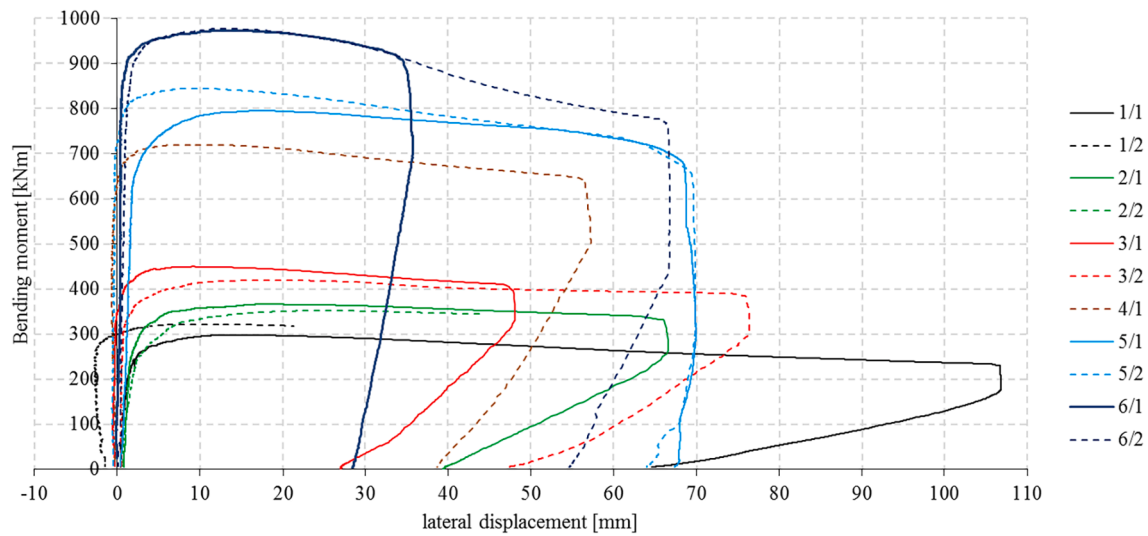


Fig. 9. Moment – lateral displacement diagrams of the middle cross-sections.

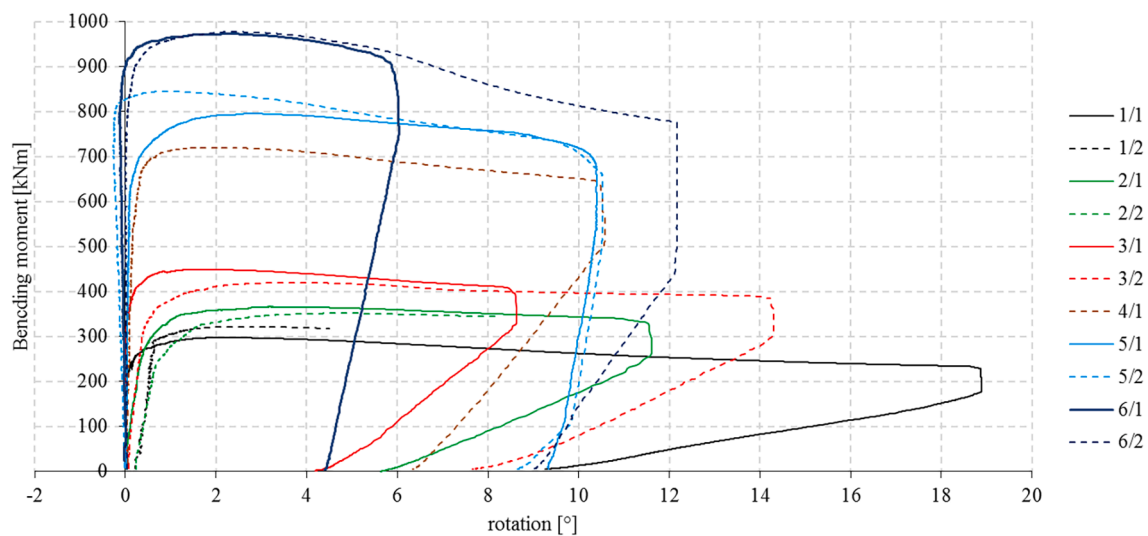


Fig. 10. Moment – rotation diagrams of the middle cross-sections.

Table 4

Theoretically calculated initial stiffness.

Specimen	I_y [cm ⁴]	EI_y [kNm ²]	$8EI_y/L^2$ [kNm/m]	M_{test} [kNm]	$e_{z,Mtest}$ [mm]
1/1	28,786	60,452	13,434	297.4	22.1
1/2	29,398	61,735	13,719	321.8	23.5
2/1	33,210	69,741	15,498	366.0	23.6
2/2	33,110	69,531	15,451	351.9	22.8
3/1	37,822	79,426	17,650	449.2	25.5
3/2	37,690	79,149	17,589	419.9	23.9
4/1	55,972	117,542	26,120	720.0	27.6
5/1	62,902	132,094	29,354	795.3	27.1
5/2	63,092	132,494	29,443	844.5	28.7
6/1	72,566	152,388	33,864	972.7	28.7
6/2	73,424	154,190	34,264	977.0	28.5

4.2. Structural behavior

Figs. 8–10 show the measured load–displacement curves of each specimen. Curves with the same color represent similar specimens (duplicated tests). In Fig. 8 the relation of the applied bending moment and measured vertical displacement in the middle cross-section is

shown. It is to be noted that the initial stiffness increases by using heavier flanges. It can be also observed that proportionally greater displacements are recovered after unloading in case of specimens with larger slenderness to lateral-torsional buckling. This phenomenon can be attributed to the rather elastic buckling of slender specimens and rather inelastic buckling of specimens having heavier flanges.

In Figs. 9 and 10 the lateral displacement curves and rotation curves of the middle cross-sections in relation with the applied bending moment are presented. For the first sight the curves look similar. It is to be noted, however, that the lateral displacement and rotation of the middle cross-sections are not necessarily developed simultaneously in the same extent. It is shown that in the case of some slender specimens (1/2, 2/1, 2/2, 3/2) the rotation can develop earlier in a greater extent which is followed by the development of additional lateral displacements before reaching the ultimate load. Furthermore, the test results prove that the magnitude and even the direction of the initial imperfection have significant effect on the ultimate load in the case of slender girders. This can be clearly seen in the case of specimens 1/1 and 1/2 where the imperfection directions are different, resulting in more than 8 % resistance increase. Moreover, it can be seen that in case of all specimens the rotations are proportionally recovered in a greater extent than

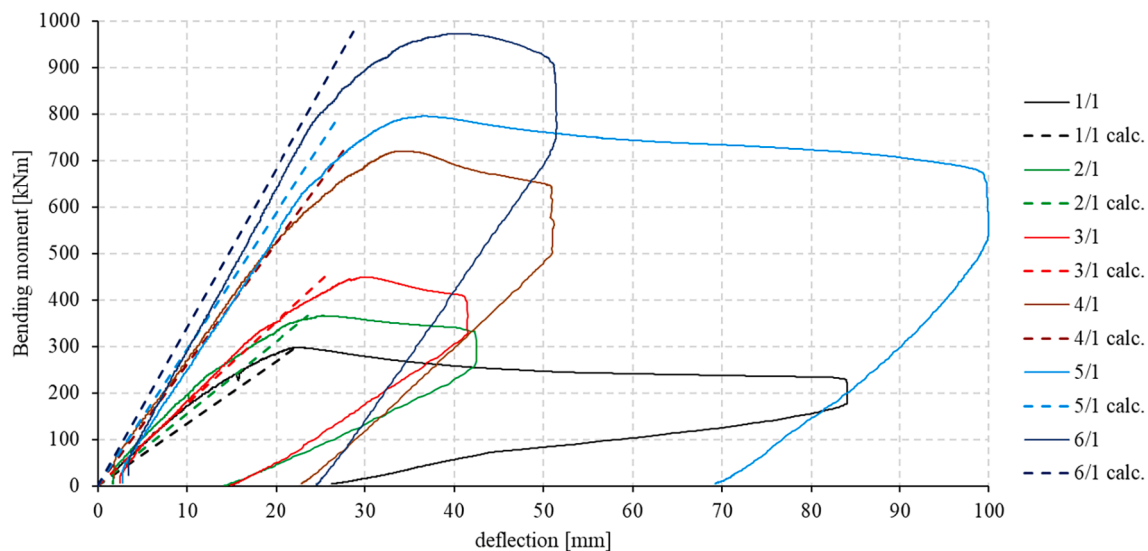


Fig. 11. Comparison of measured and calculated initial stiffnesses.

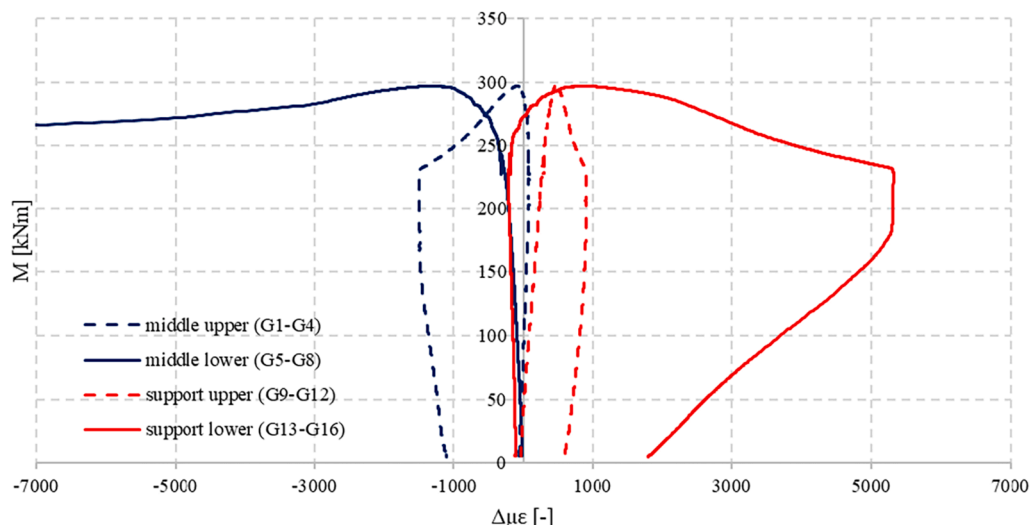


Fig. 12. Strain differences between the flange edges at the mid-span and support cross-sections of specimen 1/1.

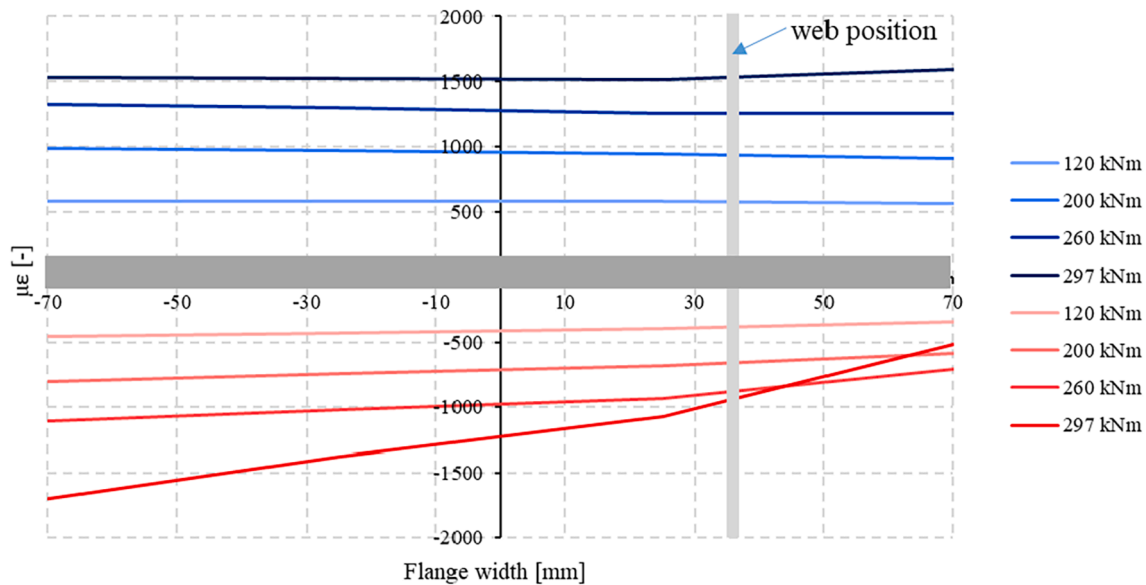


Fig. 13. Measured strain distribution in upper (blue – G1–G4 gauges) and lower (red – G5–G8 gauges) flanges in mid-span cross-section in specimen 1/1 at different load levels. (For interpretation of the references to color in this figure legend, the reader is referred to the web version of this article.)

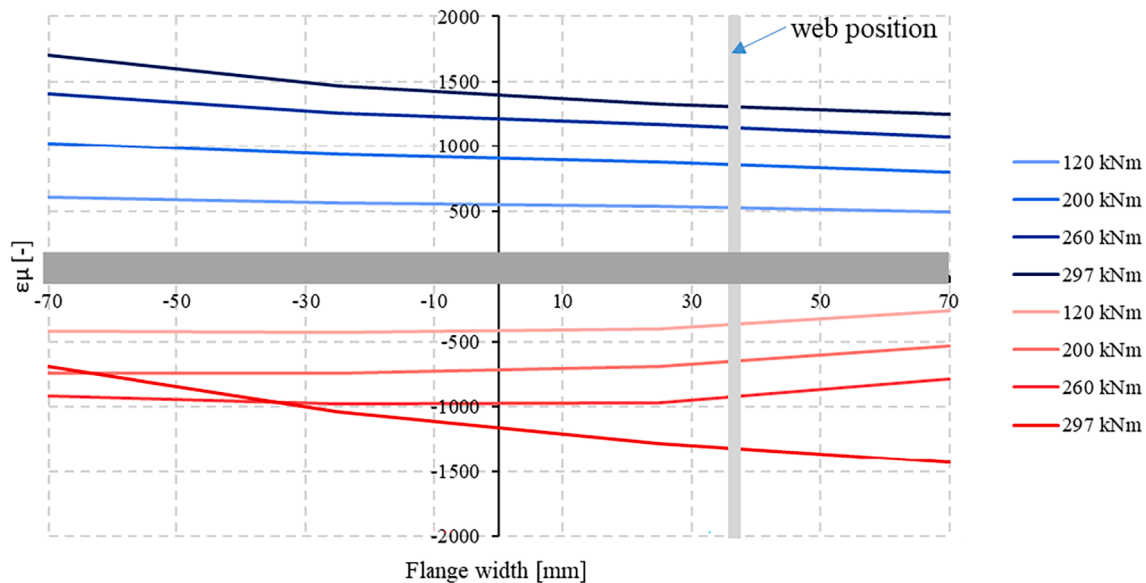


Fig. 14. Measured strain distribution in upper (blue – G9–G12 gauges) and lower (red – G13–G16 gauges) flanges at support cross-section in specimen 1/1 at different load levels. (For interpretation of the references to color in this figure legend, the reader is referred to the web version of this article.)

the lateral displacements after unloading. This confirms the previous observation that the rotation is largely allocated in elastic strains. This observation needs further investigation in the future by nonlinear FE analysis.

4.3. Initial stiffness

Table 4 collects the theoretically calculated initial stiffnesses of the specimens. Columns 4 and 6 present the calculated initial stiffnesses ($8EI_y/L^2$) and the calculated deflections associated with the measured ultimate bending moment from the tests, respectively. These calculated initial stiffnesses are plotted and compared to the moment-deflection diagrams in Fig. 11. It can be seen that the calculated initial stiffnesses shows good agreement with the measured ones.

4.4. Strain measurement

This subsection shows the strain measurement results of four specimens (1/1, 4/1, 5/2, 6/1 and 6/2). It is to be emphasized the presented strains are surface strains and not averaged membrane strains of the flanges. Figs. 12–14 present the results of specimen 1/1 where the failure is pure lateral-torsional buckling. In Fig. 12 the strain differences between the flange edges are presented in the middle (blue) and support (red) cross-sections' upper (dashed) and lower (solid) flanges. It can be seen that the strain difference ($\Delta\mu\epsilon$ – in microstrain) slightly increases in the upper and lower flanges in the elastic stage. These strain differences are the differences between results of strain gauges:

- G1 and G4 (“middle upper”),
- G5 and G8 (“middle lower”),
- G9 and G12 (“support upper”),

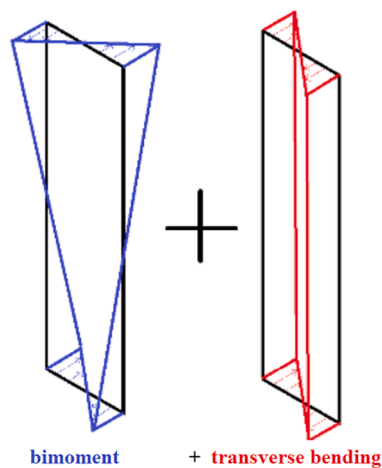


Fig. 15. Additional normal stresses from bimoment and transverse bending.

- G13 and G16 (“support lower”).

The strain difference increment in the elastic stage has a linear character. In the case of the lower flanges (solid lines) the character of the curves become nonlinear at a certain load level of around 220 kNm. After exceeding the peak (ultimate bending moment) the load level slightly drops with the development of strain differences. The strain measurement has two important observations:

- It is to be noted that the strain difference development is greater in the mid-span cross-section (blue curves) in the post-buckling range than those of at the supports (red curves). It means that at the

supports the bimoment and transverse bending moment are not fully anchored (k greater than 0.5 and k_w greater than 0.5 in Eq. (1)) otherwise the strain differences in the mid-span and at the support should be equal.

- In addition, strain differences develop in the upper flanges as well, however, the amount is small before reaching the ultimate load level which suggests that the effect of the out-of-plane rotational restraint and the warping restraint is nearly the same; meaning that the effective length factors are quasi-equal ($k \approx k_w$). For better understanding Fig. 15 presents schematically the additional normal stress distribution in the upper and lower flanges from bimoment and transverse bending from which the transverse bending moment causes the same normal stress distribution in the upper and lower flanges. After exceeding the ultimate load level the upper flange strain differences have always the same sign as the lower flange strain differences both at the mid-span and at the supports.

Figs. 13 and 14 present the distribution of the strains along the flange width in the mid-span and at the support cross-sections, respectively. The blue curves represent the upper flange strains while the red curves represent the lower flange strains at certain load levels. The strain distributions have linear character along the flange width even at higher load levels. It confirms the slightly unequal strains at the flange edges even in the elastic stage, as in Fig. 12. By increasing the load the strain differences between the flange edges increase progressively, these differences, however, are greater in the lower flange (red lines); meaning the interference of bimoment and transverse bending moment development. On the other hand in the upper flange approximately the extension of bimoment and transverse bending moment can be observed.

The same tendencies can be observed in the case of specimen type #1, #2, #3 and #4. The observations are collected below by points (i)-

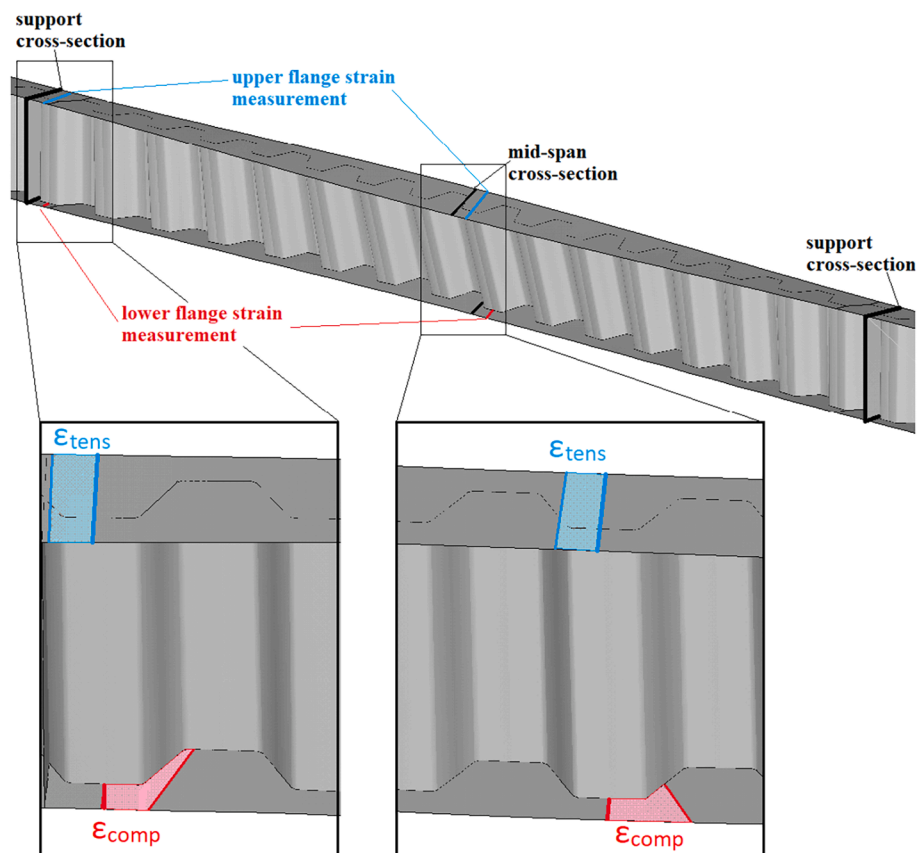


Fig. 16. Schematic drawing of deformed shape and characteristic strain distributions at mid-span and at support.

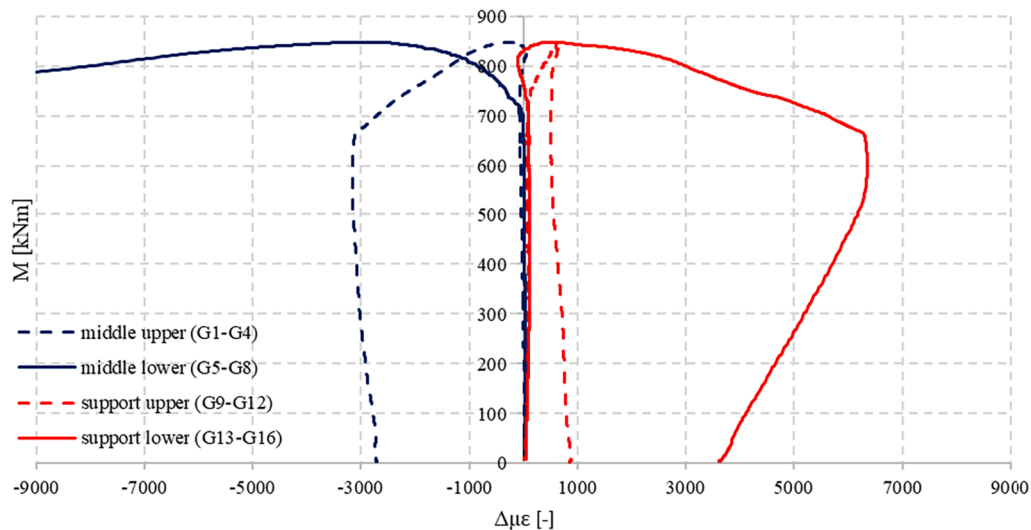


Fig. 17. Strain differences between the flange edges at the mid-span and support cross-sections of specimen 5/2.

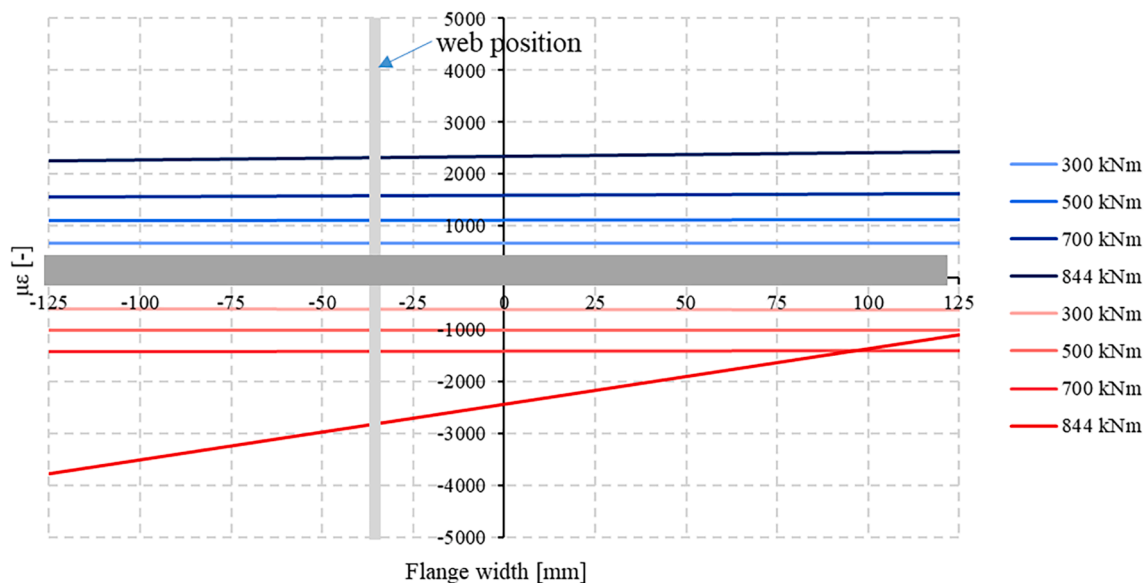


Fig. 18. Measured strain distribution in upper (blue – G1-G4 gauges) and lower (red – G5-G8 gauges) flanges in mid-span cross-section in specimen 5/2 at different load levels. (For interpretation of the references to color in this figure legend, the reader is referred to the web version of this article.)

(viii):

- (i) slight increase of strain differences $\Delta\mu\epsilon$ in the upper and lower flanges in elastic stage,
- (ii) the strain difference increment in the elastic stage has a linear character,
- (iii) character of the curves become nonlinear at a certain load level before reaching the ultimate load,
- (iv) load level slightly drops in the post-buckling range with the nearly unconstrained development of strain differences,
- (v) strain difference development is greater in the mid-span cross-section (blue curves) in the post-buckling range than those of at the support (red curves) caused by the incomplete end restraints,
- (vi) in the unloading stage the elastic strain differences are recovered ($\sim 2 \cdot f_y/E$),
- (vii) by this test arrangement the out-of-plane rotational restraint is nearly the same as the warping restraint,
- (viii) strain differences have the same sign in the lower and upper flanges after exceeding the ultimate load level.

Fig. 16 presents a schematic drawing of a typical LTB type deformed shape with the strain measurement locations at mid-span and at support. The enlarged support and mid-span cross-sections show the typical strain distributions in the upper and lower flanges at ultimate load level; the tensile strains are nearly constant in the upper flange while the compression strains are linear in the lower flange due to the development of the interference of bimoment and transverse bending moment.

Figs. 17–19 present the results of specimen 5/2 where the failure is lateral-torsional buckling and in the post-buckling range plastic flange buckling develops. It is to be noted the strain gauges G5-G8 are not in that cross-section where the plastic flange buckling occurred. In Fig. 17 the strain differences between the flange edges are presented. It can be seen that the development of local flange buckling in the post-buckling range does not result in significant change in the behavior and the observations included in points (i)–(viii) are valid.

Fig. 20 presents the local flange buckling of specimen 6/1 and 6/2. The same behavior is observed in case of specimen type #6. It can be seen the strain gauges are not in that cross-section where the visibly large flange buckling occurs, however, in the gauges's cross-section

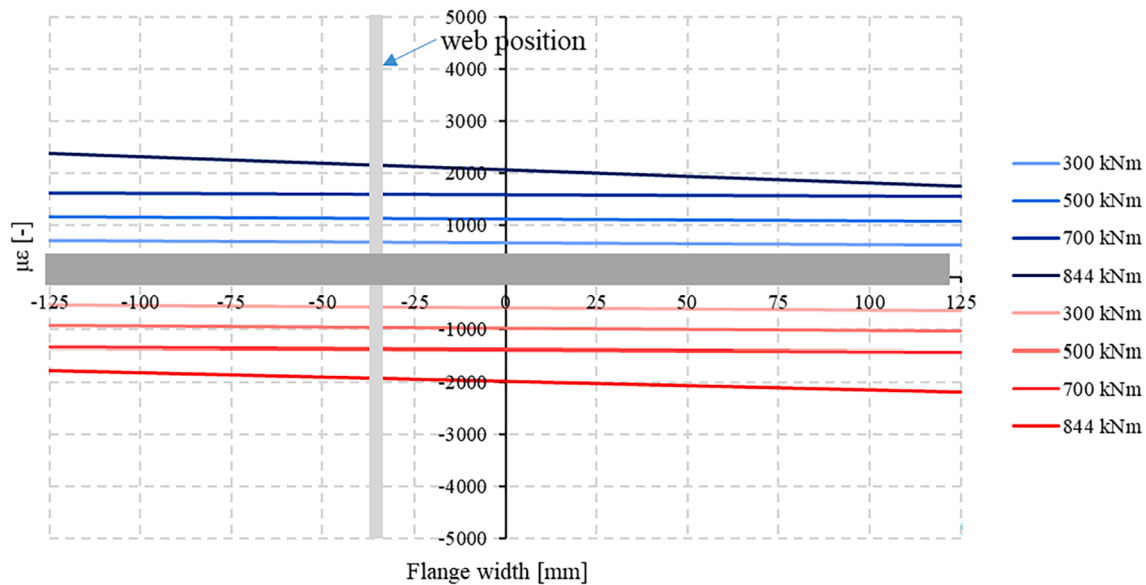


Fig. 19. Measured strain distribution in upper (blue – G9-G12 gauges) and lower (red – G13-G16 gauges) flanges at support cross-section in specimen 5/2 at different load levels. a) specimen 6/1b) specimen 6/2. (For interpretation of the references to color in this figure legend, the reader is referred to the web version of this article.)

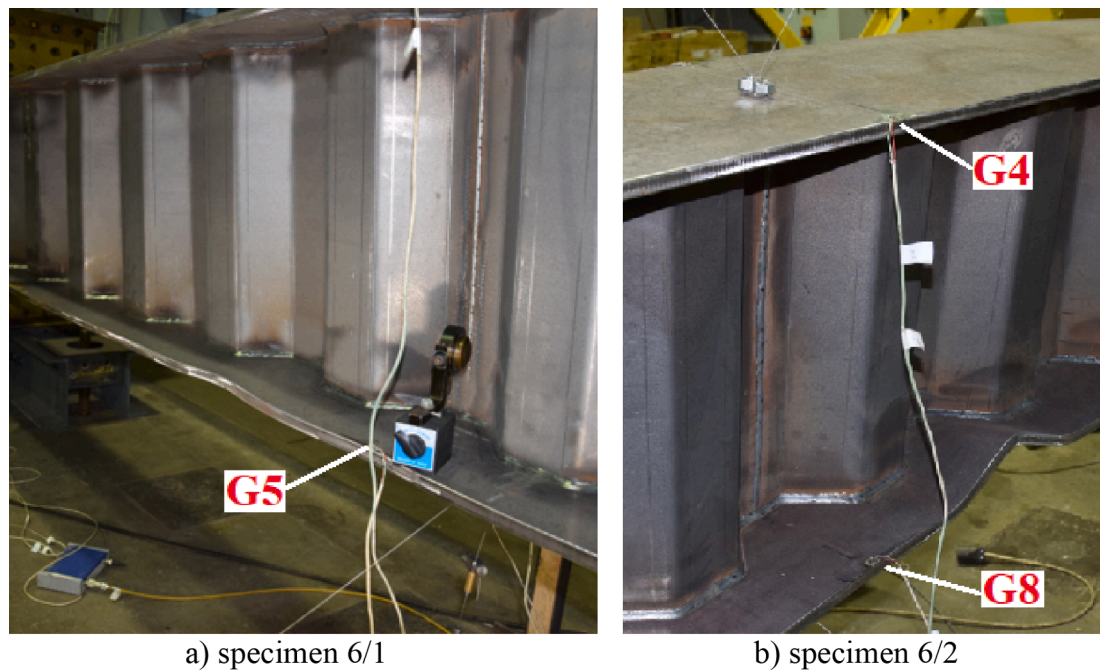
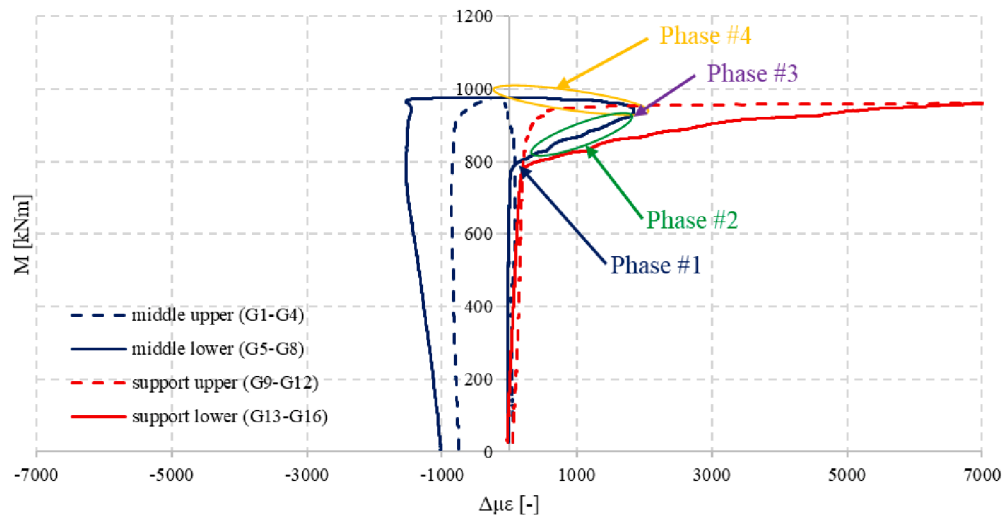


Fig. 20. Local flange buckling of specimens 6/1 and 6/2.

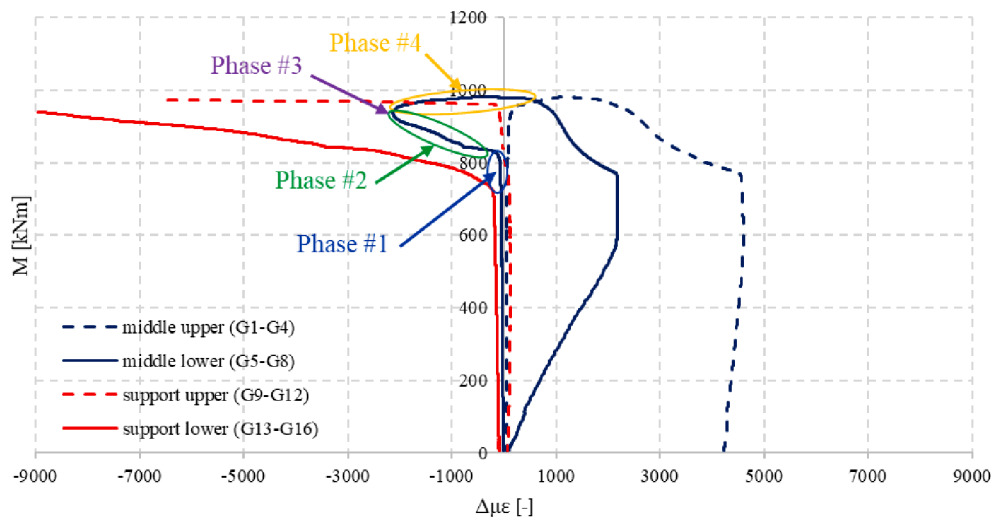
flange buckling also visibly occurs but with a smaller extent. It is to be noted the flange buckling visibly appear in the large and small flange outstands as well within the same cross-section. This is in harmony with the previous observation and identification of the authors [29] that “combined” flange buckling can develop if t_f/t_w ratio is larger than 2.5. In case of specimen type #6 this ratio is 2.67 as in case of specimen type 1TP1 and 4TP2 in [29] where these ratios are 2.59–2.75. In case of specimen type #6 only gauges G1, G4, G5 and G8 (mid-span), G9, G12, G13 and G16 (support) are placed on the flanges in the mid-span and support cross-sections.

Figs. 21–23 present the results of specimen 6/1 and 6/2 where the failure is combined local flange buckling and lateral-torsional buckling (these specimens have class 4 flanges, see in Table 3). In Fig. 21 the

strain differences are presented. It can be seen that the measured strain differences are different in case of specimen type #6 where local flange buckling occurs with lateral-torsional buckling. In the elastic stage the strain differences progressively increase in the flanges in a small extent as before in the case of other specimen types and at a certain load level the curves regarding the lower flanges become nonlinear (points (i), (ii) and (iii) are valid). When the nonlinear behavior starts the strain differences have the same sign in the lower flanges (solid lines) due to the development of local flange buckling in the mid-span cross-section. It can be observed that the strain difference increment in the lower flange is much greater at the support than in the mid-span in the pre-buckling and post-buckling ranges, too. It suggests that due to the “combined” flange buckling in upward direction: (a) the tensile strains also develop



a) specimen 6/1



b) specimen 6/2

Fig. 21. Strain differences between the flange edges at the mid-span and support cross-sections of specimen 6/1 and 6/2.

at gauge G8, besides compression strains due to lateral-torsional buckling and parallelly (b) the stiffness of mid-span cross-section decreases. At certain load levels of around 800 kNm (6/1) and 750 kNm (6/2) the combined lateral-torsional buckling (LTB) and local flange buckling (LFB) starts to develop, causing nonlinear behavior before reaching the ultimate load. These nonlinear parts have four characteristic phases depending on the governing buckling mode from point of view of the strain development:

Phase #1: additional strain differences from LTB and LFB has the same amount (in the case of specimen 6/2 it is visibly seen between load level of 750–800 kNm),

Phase #2: additional strain differences from LFB governs,

Phase #3: additional strain differences from LTB and LFB has the same amount at a certain load level,

Phase #4: additional strain differences from LTB governs.

It is to be highlighted that these are the characteristic phases in the cross-section where flange buckling occur visibly in a small extent. In the case of cross-sections having visibly large flange buckling phase #2 may dominate the whole nonlinear part before reaching the ultimate load level. The curves have a long plateau and after that the load level slightly drops in the post-buckling range when LFB and LTB are already visually

developed. Points (vii) and (viii) are also valid for specimen type #6. In the case of specimen 6/2 visually larger flange buckling occurs than in the case of specimen 6/1. As a result of this the lower flange stiffness lost is greater in specimen 6/2 which results in larger strain difference development in the mid-span upper flange, as shown by the blue dashed line in Fig. 21b. Figs. 9 and 10 confirm that the rigid body rotation and lateral displacement of specimen 6/2 starts slightly earlier than in specimen 6/1.

Figs. 22 and 23 present the distribution of the strains along the flange width in the mid-span and at the support cross-sections of specimen 6/1, respectively. When the flange buckling starts to develop (load level of 800 kNm) the strain distribution becomes strongly linear and after exceeding phase #2 (and phase #3) the strain distribution starts to get back constant (phase #4 when $\Delta\mu\epsilon = 0$) and then becomes linear again but with opposite inclination (phase #4 after exceeding $\Delta\mu\epsilon = 0$).

5. Comparison with design proposals

Fig. 24 presents the comparison of the reduction factors calculated from the test results ($\chi_{LT, test}$) to different lateral-torsional buckling curves of EN 1993-1-1 [3] ($\beta=0.75$). By the calculation of the relative

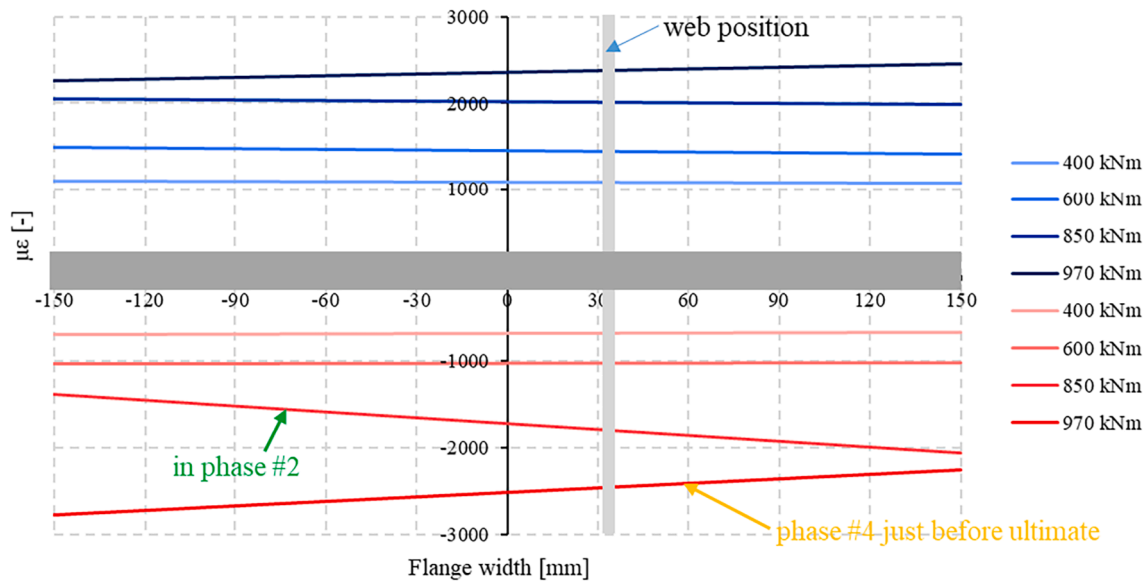


Fig. 22. Measured strain distribution in upper (blue – G1–G4 gauges) and lower (red – G5–G8 gauges) flanges in mid-span cross-section in specimen 6/1 at different load levels. (For interpretation of the references to color in this figure legend, the reader is referred to the web version of this article.)

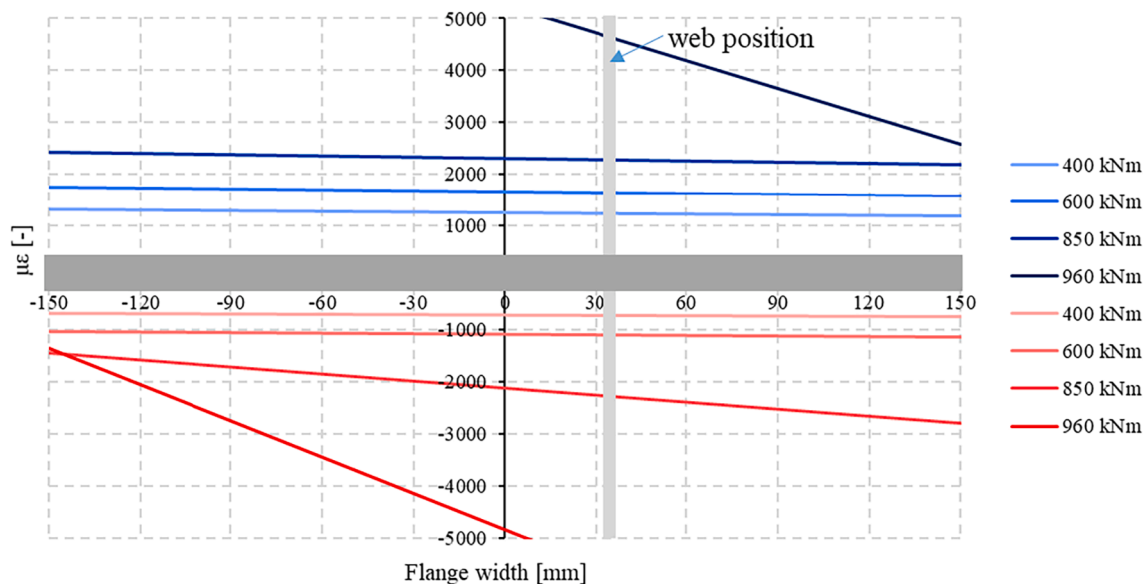


Fig. 23. Measured strain distribution in upper (blue – G9–G12 gauges) and lower (red – G13–G16 gauges) flanges at support cross-section in specimen 6/1 at different load levels. (For interpretation of the references to color in this figure legend, the reader is referred to the web version of this article.)

slenderness three different proposals for the elastic critical moment are used: (i) without any modification in the torsional or warping constants, (ii) with an additional term in the torsional constant proposed by Larsson and Persson [8] using the correction factor of Lindner [1] presented by Eq. (5), and (iii) with the slightly modified correction factor of Lindner according to Lopes et al. [11]. These calculation methods are in harmony with the “accordion effect” of corrugated web girders. In all cases the web contribution to the moment of inertias about the strong and weak axes are ignored. Since the test specimens are almost fully restrained against warping and rotation about the weak axis, both effective length factors (k_w and k) are arbitrary set to 0.5, to maximize the elastic critical moment and provide safe side solution for the buckling curve. It is to be noted all test results are above the buckling curve b and the proposal of Lopes et al. [11] gives the larger elastic critical moment and smaller relative slenderness than Larsson and Persson’s [8] solution. Table 5 presents the statistical evaluation of the results by

taking the ratio of the test and calculated lateral-torsional buckling resistances. The calculated resistances are determined according to Eq. (13) where the reduction factors (χ_{LT}) are obtained from Eqs. 6–8 using the abovementioned three different proposals for the elastic critical moment. It can be seen that the best fit and safe side solution is provided by the proposal of Lopes et al. [11] using buckling curve b . However, it should be noted that for the determination of an applicable buckling curve which fits the safety requirement of the Eurocode, a more complex statistical evaluation should be performed according to EN 1990 Annex D [33] extended by advanced FE analysis.

$$M_{b,R} = \chi_{LT} \cdot M_y \quad (13)$$

6. Conclusions

An experimental research program on the lateral-torsional buckling

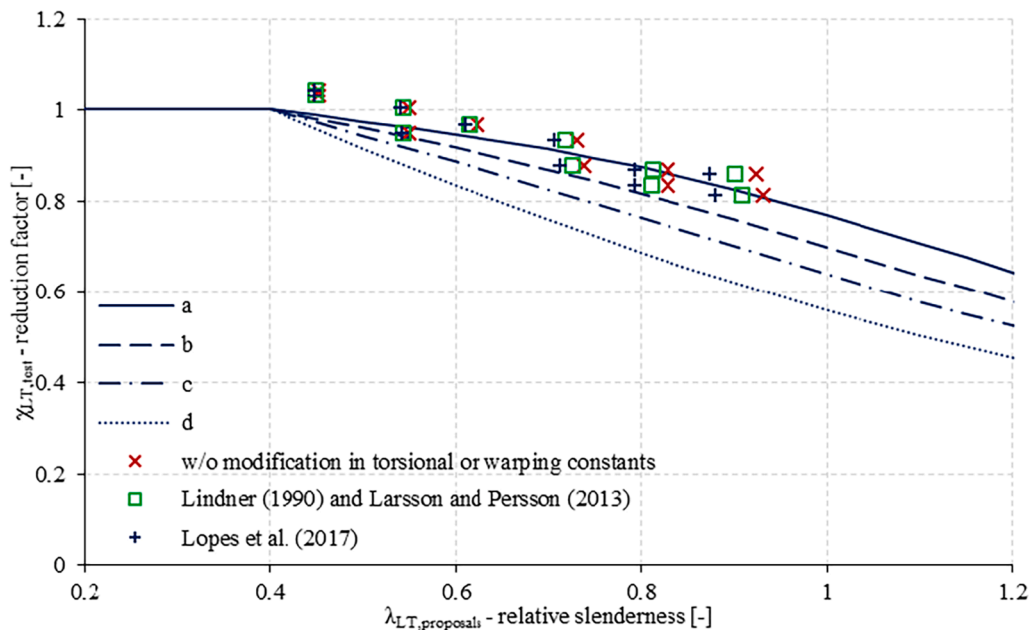


Fig. 24. Comparison of the test results and previous proposals to EN1993-1-1 buckling curves.

Table 5

Statistical evaluation of the test results and proposals using the EN1993-1-1 buckling curves.

	$M_{test}/M_{b,R,w/o\ mod}$				$M_{test}/M_{b,R,Lindner}$				$M_{test}/M_{b,R,Lopes\ et\ al.}$			
	a	b	c	d	a	b	c	d	a	b	c	d
Average	1.020	1.070	1.124	1.216	1.014	1.061	1.113	1.201	1.008	1.053	1.102	1.186
Std. Dev.	0.030	0.036	0.060	0.107	0.031	0.032	0.052	0.097	0.034	0.028	0.044	0.084
CoV	0.030	0.033	0.053	0.088	0.031	0.030	0.047	0.081	0.034	0.027	0.040	0.071
Min	0.970	1.011	1.038	1.083	0.962	1.008	1.034	1.079	0.952	1.007	1.032	1.076
Max	1.057	1.152	1.253	1.419	1.056	1.131	1.227	1.385	1.056	1.108	1.197	1.346

strength of trapezoidally corrugated web girders is presented. Based on the experimental study the following conclusions are drawn:

- for girders having compact flanges pure lateral-torsional buckling failure occur, while in the case of girders having slender flanges the flange buckling failure couples with lateral-torsional buckling failure;
- the failure modes are rigid cross-sectional movement, no distortional type failure of the web can develop;
- proportionally larger displacements are recovered after unloading for slender specimens attributing to rather elastic buckling, and rather inelastic buckling of specimens with heavier flanges can occur;
- the initial imperfections have significant resistance reduction effect on the lateral-torsional buckling strength;
- for this test arrangement rotational and warping restraint at the supports are incomplete since k and k_w may be slightly greater than 0.5, meaning that the evaluation is on the safe side;
- the lateral-torsional buckling curve b of EN1993-1-1 [2] (with $\beta = 0.75$ and $\lambda_{LT,0} = 0.4$, and using $k = k_w = 0.5$ as safe side approximation) gives lower bound estimate for the prediction of the lateral-torsional buckling strength of trapezoidally corrugated web girders;
- the proposal of Lopes et al. [11] for the determination of the elastic critical moment provides the best solution together with the lateral-torsional buckling curve b of EN1993-1-1 [2] based on the current test results.

Further investigations are needed on the effective length factors determination to find the best fit buckling curve. Additional numerical

simulation results and a more complex statistical evaluation should be also performed to determine the reliable buckling curve for the prediction of the lateral-torsional buckling strength of trapezoidally corrugated web girders which fits to the requirement of EN 1990 [32].

Declaration of Competing Interest

The authors declare that they have no known competing financial interests or personal relationships that could have appeared to influence the work reported in this paper.

Acknowledgments

The presented research program is part of the “BridgeBeam” R&D project No. GINOP-2.1.1-15-2015-00659; the financial support is gratefully acknowledged. Furthermore the research was also supported by the fx1 ÚNKP-19-3 New National Excellence Program of the Ministry for Innovation and Technology scholarship of the first author; the financial support is gratefully acknowledged. The research work was also supported by the Grant MTA-BME Lendület LP2021-06 / 2021 “Theory of new generation steel bridges” program of the Hungarian Academy of Sciences.

References

- [1] Lindner J. Lateral torsional buckling of beams with trapezoidally corrugated webs, Proceedings of the 4th International Colloquium on Stability of Steel Structures, Budapest, Hungary, 79-82, 1990.
- [2] EN 1993-1-1:2005, EUROCODE 3: Design of steel structures, Part 1-1: General rules and rules for buildings.

- [3] Timoshenko SP, Gere JM. Theory of elastic stability. 2nd ed. London: McGraw-Hill; 1961.
- [4] Sayed-Ahmed EY. Lateral torsion-flexure buckling of corrugated web steel girders. Proceedings of the Institution of Civil Engineers - Structures and Buildings 2005; 158(1):53–69.
- [5] Moon J, Yi J-W, Choi BH, Lee H-E. Lateral-torsional buckling of I-girder with corrugated webs under uniform bending. Thin-Walled Struct 2009;47(1):21–30.
- [6] Nguyen ND, Kim SN, Han S-R, Kang Y-J. Elastic lateral-torsional buckling strength of I-girder with trapezoidal web corrugations using a new warping constant under uniform moment. Eng Struct 2010;32(8):2157–65.
- [7] Zhang Z, Li G, Sun F. Flexural-torsional buckling of H-beams with corrugated webs. Adv Mater Res 2011;163–167:351–7.
- [8] Larsson M, Persson J. Lateral-torsional buckling of steel girders with trapezoidally corrugated webs, MSc thesis, Gothenburg, Sweden, 57, 2013.
- [9] Ilanovsky V. Assessment of bending moment resistance of girders with corrugated web. Pollack Periodica 2015;10(2):35–44.
- [10] Ibrahim SA. Lateral torsional buckling strength of unsymmetrical plate girders with corrugated webs. Eng Struct 2014;81:123–34.
- [11] Lopes GC, Couto C, Real PV, Lopes N. Elastic critical moment of beams with sinusoidally corrugated webs. J Constr Steel Res 2017;129:185–94.
- [12] Guo C, Papangelis J. Torsion of beams with corrugated webs, Proceedings of the Ninth International Conference on Advances in Steel Structures (ICASS'2018), Hong Kong, China, 5–7 December, 373–382, 2018.
- [13] Kazemi nia korrani HR. Lateral bracing of I-girder with corrugated webs under uniform bending. J Constr Steel Res 2010;66(12):1502–9.
- [14] Nguyen ND, Han S-R, Lee G-S, Kang Y-J. Moment modification factor of I-girder with trapezoidal-web-corrugations considering concentrated load height effects. J Constr Steel Res 2011;67(11):1773–87.
- [15] Nguyen ND, Han SR, Kang YJ. Lateral-torsional buckling of tapered I-girder with corrugated webs, The 6th International Symposium on Steel Structures, November 3–5, Seoul, Korea, 627–634, 2011.
- [16] Nguyen ND, Han SR, Kim JH, Kim SN, Kang YJ. Moment modification factors of I-girders with trapezoidal web corrugations under moment gradient. Thin-Walled Struct 2012;57:1–12.
- [17] Moon J, Lim NH, Lee HE. Moment gradient correction factor and inelastic flexural-torsional buckling of I-girders with corrugated steel webs. Thin-Walled Struct 2013;62:18–27.
- [18] Kubo M, Watanabe K. Lateral-torsional buckling capacity of steel girders with corrugated web plates. Doboku Gakkai Ronbunshuu A 2007;63(1):179–93.
- [19] Elkawas AA, Hassanein MF, El Hadidy AM, El-Boghdadi MH, Elchalakani M. Behaviour of corrugated web girders subjected to lateral-torsional buckling: Experimental tests and numerical modelling. Structures 2021;33:152–68.
- [20] Hannebauer D. Zur Querschnitts- und Stabtragfähigkeit von Trägern mit profilierten Stegen, PhD dissertation, Brandenburgischen Technischen Universität, Cottbus, Germany, 2008.
- [21] Pimenta RJ, Queiroz G, Diniz SMC. Reliability-based design recommendations for sinusoidal-web beams subjected to lateral-torsional buckling. Eng Struct 2015;84: 195–206.
- [22] Zhang Z, Pei S, Qu B. Cantilever welded wide-flange beams with sinusoidal corrugations in webs: Full-scale test and design implications. Eng Struct 2017;144: 163–73.
- [23] Hassanein MF, Elkawas AA, Shao Y-B, Elchalakani M, El Hadidy AM. Lateral-Torsional buckling behaviour of mono-symmetric S460 corrugated web bridge girders. Thin-Walled Struct 2020;153:106803.
- [24] Elkawas AA, Hassanein MF, Elchalakani M. Lateral-torsional buckling strength and behaviour of high-strength steel corrugated web girders for bridge construction. Thin-Walled Struct 2018;122:112–23.
- [25] Shao Y-B, Zhang Y-M, Hassanein MF. Strength and behaviour of laterally-unrestrained S690 high-strength steel hybrid girders with corrugated webs. Thin-Walled Struct 2020;150:106688.
- [26] Hassanein MF, Elkawas AA, Shao Y-B. Assessment of the suitability of eurocode design model for corrugated web girders with slender flanges. Structures 2020;27: 1551–69.
- [27] Jäger B, Dunai L. Nonlinear imperfect analysis of corrugated web beams subjected to lateral-torsional buckling. Eng Struct 2021;245:112888.
- [28] ISO 6892-1:2016, Metallic materials – Tensile testing – Part 1: Method of test at room temperature.
- [29] Jäger B, Dunai L, Kövesdi B. Flange buckling behavior of girders with corrugated web – Part I: Experimental study. Thin-Walled Struct 2017;118:181–95.
- [30] Jäger B, Dunai L, Kövesdi B. Flange buckling behavior of girders with corrugated web – Part II: Numerical study and design method development. Thin-Walled Struct 2017;118:238–52.
- [31] EN 1993-1-5:2005, EUROCODE 3: Design of steel structures. Part 1-5: Plated structural elements.
- [32] EN 1990:2005, Eurocode – Bases of structural design.